Materials Advances

ROYAL SOCIETY OF CHEMISTRY

PAPER

View Article Online
View Journal

Cite this: DOI: 10.1039/d5ma01349f

Carbon-supported NiS catalysts for sustainable transfer-hydrogenation reactions of nitroarenes

Ankit Kumar,[a] Pascal A. Roll,[a] Anna Stephan,[a] Claus Feldmann,[a] Arjun Neyyathala,[a] Paolo Dolcet[b] and Schirin Hanf *[a]

Received 20th November 2025,
Accepted 1st April 2026

DOI: 10.1039/d5ma01349f

rsc.li/materials-advances

We report Ni_3S_2/C as an effective and environmentally friendly catalyst for the transfer hydrogenation of nitroarenes, using hydrazine monohydrate as a hydrogen donor under mild reaction conditions. The catalyst achieves complete conversion and excellent selectivity across a wide range of nitrobenzene derivatives, bearing both electron-withdrawing and electron-donating groups. Mechanistic studies indicate mainly a direct reduction pathway from nitrobenzene to aniline *via* nitrosobenzene, unlike Ni/C, which favours a condensation route. The incorporation of sulphur into Ni is shown to tune the selectivity and enhance sulfur tolerance, thereby enabling efficient hydrogenation of nitroarenes containing thiol groups. Moreover, Ni_3S_2/C is recyclable and effective on a gram-scale reaction, maintaining full conversion and high aniline yields. Compared to conventional noble- and non-noble-metal catalysts that require high-pressure molecular hydrogen, this system offers a cost-effective, robust, and sustainable alternative with strong potential for industrial-scale applications.

1. Introduction

Aniline and its derivatives are crucial intermediates in the production of fine chemicals, such as pharmaceuticals, agrochemicals, dyes, and polymers.[1,2] Due to their high industrial demand, the development of cost-effective and sustainable methods for the synthesis of aniline and related compounds from readily available raw materials remains a key focus. The catalytic hydrogenation of nitroarenes has been a key method for producing aniline and its derivatives for over a century, valued for its operational simplicity, environmental compatibility, and adaptability to both laboratory- and industrial-scale applications.[3–5] Traditionally, the hydrogenation of organic compounds has been carried out either through direct hydrogenation using molecular hydrogen[6–11] or *via* catalytic transfer hydrogenation reactions,[12–17] in which hydrogen is provided by alternative donor molecules instead of gaseous hydrogen. However, conventional hydrogenation methods face several challenges, including the high cost of hydrogen compression, transportation difficulties, safety risks, and the need for complex reactor systems with strict operating conditions.[18–20] As a result, transfer hydrogenation reactions have gained significant attention, due to their operational simplicity, reduced equipment requirements, and the gradual and controlled release of hydrogen during the catalytic reactions.[18–20] Transfer hydrogenation reactions commonly employ metal hydride reagents, such as sodium borohydride ($NaBH_4$) and lithium aluminium hydride ($LiAlH_4$). However, these approaches suffer from several drawbacks, including a high reagent consumption, poor atom economy, substantial metal salt waste generation, and complex product separation procedures.[21,22] These drawbacks, together with the high cost of metal hydride reagents at industrial scales, significantly limit their practical application in selective hydrogenation reactions. Consequently, recent research has shifted towards the development of alternative hydrogen sources, like formic acid, alcohols, amine–boranes and hydrazine monohydrate, as more stable derivative to anhydrous hydrazine.[12–17,23] Hydrazine monohydrate is particularly attractive for transfer hydrogenation reactions because it allows transformations to be carried out under mild, pressure-free conditions. By eliminating the need for high-pressure hydrogen gas and specialized equipment, it simplifies laboratory-scale studies, facilitates mechanistic investigations, and enables rapid catalyst screening. Although its large-scale application is limited by toxicity and handling concerns, hydrazine monohydrate remains a valuable and well-established model hydrogen donor. In contrast, molecular hydrogen is generally preferred for industrial processes because of its clean by-product profile and the availability of established infrastructure.

To selectively activate hydrazine monohydrate and control its decomposition into nitrogen and hydrogen under mild reaction conditions, various metal-based catalytic systems have been developed.[24,25] Currently, both homogeneous and

[a] Institute of Inorganic Chemistry, Karlsruhe Institute of Technology, Engesserstr. 15, 76131 Karlsruhe, Germany. E-mail: Schirin.hanf@kit.edu
[b] Department of Chemical Sciences, University of Padova, Via Francesco Marzolo 1, Padova 35131, Italy

heterogeneous catalysts are employed in transfer hydrogenation reactions. However, heterogeneous catalysts offer distinct advantages over their homogeneous counterparts, particularly in terms of catalyst separation and recovery.[26,27] In this context, noble metal-based heterogeneous catalysts, such as Ru-OMC-800 (OMC: ordered mesoporous carbon),[28] Ru/PNC-700 (PNC: phosphorous- and nitrogen-doped carbon),[29] Ru/MoS_2,[30] Ir-MoOx/SiO_2,[31] Pd/CeO_2,[32] Pd/C,[33] Pt/CeO_2,[34] ZrO_2@Pt,[35] Pt/TiO_2/SBA-15,[36] and Rh/COF (COF: covalent organic framework),[37] have been explored. An overview is given in Table S1. While these catalysts exhibit excellent catalytic activity, their poor selectivity, high cost, and limited availability restrict their application in large-scale industrial applications.

To address these limitations, non-noble-metal-based heterogeneous catalysts have been developed for the chemoselective transfer hydrogenation of nitroarenes (Table S1). For example, iron-based materials, such as Fe@C,[38] $FeCeO_2$,[39] Fe_2O_3/LRC-700 (LRC: lignin-derived carbon),[40] and Fe–Fe_3C–Fe_3O_4@CN (CN: nitrogen-doped carbon),[41] as well as immobilized Fe in ionic liquids,[42] and ultrasmall FeS_2 nanoparticles,[43] have demonstrated quantitative conversion and excellent selectivity toward anilines, typically using hydrazine monohydrate as the hydrogen source. Also, nickel-based catalysts, such as Ni/TiO_2,[44] Ni/C_{60},[45] Ni–NC-700,[46] Ni_2P/AC (AC: activated carbon),[47] and Ni/SiO_2,[48] have been reported in this context. For example, Sharma *et al.* developed Ni_2P/AC nanocomposites and demonstrated their catalytic activity in the reduction of aromatic nitro compounds.[47] Using hydrazine monohydrate as the hydrogen source at 70 °C, complete conversion of nitrobenzene (100%) and 93% yield of aniline were achieved in 2 h. Jiang *et al.* prepared highly dispersed Ni nanoparticles on SiO_2 (Ni/SiO_2) *via* atomic layer deposition. Under hydrazine-assisted hydrogenation conditions at 100 °C, an aniline yield of 45% was obtained after 2 h, which increased to 94% after 8 h reaction time.[48] In parallel, copper-based systems (Cu/Celite),[49] and a variety of cobalt-based architectures, ranging from supported nanoparticles to single-atom catalysts embedded in N-doped carbon matrices, such as Co@NC,[50] Co@NC/AC,[51] Co@NCT (NCT: nitrogen-doped carbon nanotube),[52] Co@C-800-AL,[53] Co-L@C-800,[54] Co/NPC,[55] Co/MA-800 (MA: macroalgae-derived carbon),[56] Co@C/CNT,[57] and Co@NC-600,[58] have enabled efficient nitroarene reduction, employing alternative hydrogen donors such as methanol or formic acid. Despite these advances, many reported systems rely on elevated temperatures, long reaction times, or highly specific reaction environments. For instance, Dey *et al.* investigated a single-atom cobalt catalyst (Co@C-800-AL) for the transfer hydrogenation of nitroarenes using methanol as the hydrogen source. For nitrobenzene, complete conversion and 95% yield of aniline were achieved at 140 °C in 24 h with Cs_2CO_3 as base.[53]

The catalytic performance of these non-noble metal catalysts can be structurally and electronically tuned by the incorporation of p-block elements to form alloys or intermetallic compounds. Here, the formation of isolated active metal sites, in analogy to the well-known concept of frustrated single sites in homogenous catalysis, has been proposed.[59] In this context, metal phosphides and sulphides have demonstrated very promising catalytic activity. For example, metal phosphides (M_xP_y; M = Ni, Co, Ru, Pd, and Pt) have been applied in hydrogenation reactions,[60] water splitting,[61] coupling[62] and oxidation reactions,[63] as well as the deoxygenation of sulfoxides.[64] Similarly, metal sulphides, such as MoS_2, WS_2, RuS_2, PdS_x, and RhS_x, have shown efficiency in hydrodesulfurization reactions,[65] CO_2 hydrogenation,[66] and hydroformylation reactions.[67] Although sulphur is typically considered to be a catalyst poison in heterogeneous catalysis,[68] sulphide-based catalysts (*e.g.*, MoS_2, Co–Mo–S, and Ru–W–S) have successfully been employed in the hydrogenation of sulphur-containing nitroaromatic compounds. For instance, Corma *et al.* developed a Co–Mo–S catalyst capable of hydrogenating 4-nitrothioanisole to 4-aminothioanisole with complete conversion at 150 °C under 11 bar H_2.[69] More recently, Glorius *et al.* reported a Ru–W–S catalyst for the hydrogenation of sulphur-containing quinolines to tetrahydroquinolines.[70] Zhang *et al.* synthesized a Pd_xS_y/C catalyst *in-situ* for the hydrogenation of sulphur-containing nitroarenes to the corresponding amines.[71] Similarly, Yu *et al.* explored Pd_4S nanoparticles supported on sulphur-doped carbon (Pd_4S/SC) for the selective hydrogenation of 4-chloronitrobenzene at 80 °C under 6 bar H_2.[72] Despite the high activity and selectivity of the before-mentioned catalysts, their reliance on high-pressure molecular hydrogen poses sustainability and safety challenges.

Building on the successful p-block/d-metal element combination strategy, we report the synthesis of a nickel sulphide-based catalyst (Ni_3S_2/C) for the transfer hydrogenation of nitroarenes. Ni_3S_2/C was employed under base-free conditions using hydrazine hydrate as the hydrogen source, thereby avoiding the need for molecular hydrogen. At this point, it is important to note that hydrazine monohydrate is toxic, corrosive, and potentially carcinogenic. Therefore, its handling requires strict safety measures, including the use of appropriate personal protective equipment (PPE), working in a well-ventilated fume hood, and adherence to institutional safety protocols. The reaction conditions were systematically optimised to maximise the product yield by varying key parameters. This work highlights the potential of nickel sulphide-based catalysts in sustainable organic transformations and opens avenues for large-scale applications in the chemical industry.

2. Experimental section

2.1. Reagents

Nickel chloride hexahydrate (Sigma-Aldrich, >98%), thiourea (Sigma-Aldrich, 99%), carbon (BASF SE), ZrO_2 (BASF SE), Al_2O_3 (BASF SE), SiO_2 (Cariact), hydrazine monohydrate (TCI, >98%), *n*-heptane (TCI, >99%), ethyl acetate (Fischer Scientific, 98%), *n*-decane (abcr, >99%), methanol (VWR, 99.8%), ethanol (Carl Roth, >99.5%), formic acid (Merk, 91%), nitrobenzene (Merck, >99%), (TCI, 98%), 2-chloronitrobenzene (TCI, 99%), 4-chloronitrobenzene (TCI, >98%), 2-nitrophenol (TCI, 98%), 4-nitrophenol (TCI, >99%), 4-nitrotoluene (TCI, >99%), 2-nitroanisole (TCI, >98%), 4-nitroanisole (>98%), 4-nitrobenzonitrile (TCI, 98%), 4-fluoronitrobenzene (TCI, >98%), 1,4-dinitrobenzene (TCI,

99%), 4-nitrothioanisole (abcr, 98%), 4-nitrophenyl phenyl sulphide (Thermo Scientific, 98%), 4-nitrothiophenol, 4-nitrobenzenethiol (TCI, >95%), nitroso benzene (TCI, 98%), and azobenzene (TCI, >98%) were purchased and used without any further purification. For the thermal treatment during catalyst synthesis, 5%H_2/N_2 (99.999%) was used and purchased from Air Liquide.

2.2. Characterisation

Powder X-ray diffraction (PXRD) measurements were carried out using a Stoe STADI-MP diffractometer operating with a Ge-monochromatized Cu K_α radiation (λ = 1.541 Å) in transmission mode. For the measurements, about 5–10 mg of sample was placed between thin films of scotch tape and acetate paper, which were then placed into the sample holder. The measurements were carried out in the range of 2 to 92° with a step size of 3°. The shape, size, and chemical composition of the Ni_3S_2/C sample were studied by high-angle annular dark-field (HAADF) scanning transmission electron microscopy (STEM) combined with energy-dispersive X-ray spectroscopy (EDXS). The experiments were conducted with a FEI Tecnai Osiris microscope at 200 keV electron energy, which is equipped with a Super-X EDXS system comprising four silicon drift detectors. EDXS elemental maps were recorded and used to investigate the element distribution within the respective sample. The maps were analysed using the ESPRIT software (version 2.3) from Bruker. For the sample preparation, the solid sample was dispersed in ethanol under ultrasonication and then deposited over the amorphous carbon-coated 400 mesh Cu grid and dried under vacuum at 80 °C overnight. Thermogravimetric analysis (TGA) of the carbon support and the Ni_3S_2/C catalyst was performed over a temperature range of 30–1200 °C under air at a heating rate of 5 K min^{-1} using a NETZSCH STA 449 F3 Jupiter instrument. Raman spectroscopy was performed with an inVia Raman spectrometer (Renishaw) equipped with a frequency doubled Nd:YAG laser (532 nm, 100 mW) and a 50× Leica DM2500 optical microscope. A laser power of 10% was employed together with a 600 lines per mm grating. Spectra were recorded from 6 different points with an acquisition time of 30 s. All obtained spectra for each sample were converged. The software WiRE 4.4 (Renishaw) was used for the data treatment. X-ray photoelectron spectroscopy (XPS) was performed with a Thermo Scientific Escalab QXi. The spectra were collected employing a monochromatic Al K_α source (λ = 1486.6 eV), with a spot size of 650 μm and using a flood gun for charge compensation. For the XPS measurements, the catalyst was stored under an inert atmosphere in a glove box and immediately transferred to the XPS instrument with minimal exposure to air. The measurements were performed without any additional pretreatment. The survey spectra were collected (0–1350 eV) with a pass energy of 100 eV and a step size of 1 eV, whereas detailed regions were collected with a pass energy of 20 eV and a step size of 0.05 eV. The specific surface area was measured by N_2 physisorption using the Brunauer–Emmett–Teller (BET) method. The measurements were carried out with an AUTOSORB IQ-XR VITON analyzer (Anton Paar). The samples were treated at 150 °C for 3 h under reduced pressure before the measurement. The metal loading of the catalyst was determined *via* inductive coupled plasma optical emission spectroscopy (ICP-OES) measurements using an iCAP7600 DUO from Thermo-Fisher-Scientific. Before analysis, the samples were digested using acids and high pressure.

2.3. Catalyst syntheses

Nickel sulphide nanoparticles supported on carbon (Ni_3S_2/C) were synthesized *via* a wet impregnation method followed by thermal treatment. For the preparation of a 10 wt% Ni catalyst, 225 mg of carbon (finely ground) was dispersed in 15 mL of distilled water in a 50 mL round-bottom flask and sonicated for 20 minutes. Subsequently, $NiCl_2{\cdot}6H_2O$ (0.425 mmol) and thiourea (2.55 mmol) were added to the suspension, and the mixture was stirred at room temperature for 2 h. The mixture was then heated at 70 °C overnight to remove the solvent completely. The resulting precursor was subjected to thermal treatment at 400 °C under a continuous flow of 5% H_2/N_2 gas at a heating rate of 5 °C min^{-1} for 4 h to obtain the Ni_3S_2/C catalyst. Similarly, other supported catalysts (Ni_3S_2/ZrO_2, Ni_3S_2/Al_2O_3 and Ni_3S_2/SiO_2) were also synthesized. For comparison, a reference Ni/C catalyst (10 wt% Ni) was prepared using the same procedure, excluding the addition of thiourea, and applying a slightly modified thermal treatment (500 °C, 5 °C min^{-1}, 5 h).

2.4. Catalytic testing

The catalytic performance was evaluated using nitrobenzene as model substrate. In a typical catalytic test, nitrobenzene (0.97 mmol, 100 μL), *n*-heptane (2 mL), and the catalyst (30 mg) were placed in a 25 mL Schlenk round-bottom flask. It is important to note that the size of the flask has an impact on the performance of the catalysts, since it affects the gas atmosphere of the head space. The mixture was sonicated for several minutes to ensure the homogeneous dispersion of the catalyst. Subsequently, hydrazine monohydrate (10 equiv.) was added, the flask was sealed with a stopper, and the Schlenk valve was closed. The reaction mixture was then heated to 70 °C in a preheated oil bath and stirred at 600 rpm for the desired reaction time. After completion of the reaction, the Schlenk valve was carefully opened to release any gas generated during the reaction, and subsequently the mixture was allowed to cool to room temperature. Ethyl acetate (2 mL) and *n*-decane (50 μL, used as an external standard) were added, and the resulting biphasic mixture was thoroughly mixed. The organic phase was then filtered through a 0.2 μm syringe filter, and 100 μL of the filtrate was diluted with 900 μL of methanol or ethyl acetate to obtain a homogeneous solution for further analysis. Product identification and quantification was performed using an Agilent GC-MS system comprising a 8860 GC system coupled with a 5977B mass selective detector (MSD). From the GC vial, 1 μL was automatically injected into the GC-MS system at a plunger speed of 1000 μL min^{-1}, using a split ratio of 100 : 1 and an injection temperature of 300 °C. Chromatographic separation was achieved using a fused silica capillary column (inner diameter: 0.25 mm; film thickness: 0.25 μm; length: 30 m). The oven temperature program was as follows: initial hold at

50 °C for 2.25 min, ramping at 25 °C min^{-1} to 250 °C for 2 min, followed by a final hold at 300 °C for 1.0 min.

2.5. Recyclability studies

The catalytic reaction was performed as specified before. After the completion of the reaction, the catalyst was recovered from the reaction mixture by centrifugation, washed three times with ethyl acetate and acetone, dried overnight at 60 °C, and then reused for the next catalytic run.

2.6. Gram scale reaction

To a 100 mL Schlenk round-bottom flask, nitrobenzene (19.4 mmol), Ni_3S_2/C (600 mg), *n*-heptane (40 mL), and hydrazine monohydrate (10 equiv.) were added and stirred at 70 °C at 600 rpm for the specified time. After completion, the reaction mixture was cooled to room temperature. Ethyl acetate (40 mL) and *n*-decane (1 mL, used as an external standard) were added to the reaction mixture. The organic phase of the mixture was then filtered through a 0.2 μm syringe filter, and 100 μL of the filtrate was diluted with 900 μL of ethyl acetate to prepare a homogeneous solution for further product analysis *via* GC-MS.

3. Results and discussion

3.1. Catalyst characterisation

Nickel sulphide nanoparticles supported on carbon (Ni_3S_2/C) were synthesized *via* a wet impregnation method followed by a thermal treatment. To prepare a 10 wt% Ni-based catalyst, nickel chloride and thiourea (in a 1 : 6 molar ratio) were added to a carbon suspension in demineralised water. The mixture was stirred at room temperature for 2 h. The as-prepared material was then dried overnight and thermally treated under a continuous flow of 5% H_2 in N_2 to form the Ni_3S_2/C catalyst. Similarly, Ni/C (10 wt% Ni) was prepared as the reference catalyst using the same procedure, excluding the addition of thiourea, and applying a slightly modified thermal treatment (500 °C, 5 °C min^{-1}, and 5 h). The thermal treatment conditions were intentionally selected based on the distinct chemical requirements of each catalyst system. For the Ni_3S_2/C catalyst, the thermal treatment at 400 °C (5 °C min^{-1}, 4 h) was applied to promote the controlled sulfidation and stabilization of the Ni_3S_2 phase. Higher temperatures or stronger reducing environments can induce sulphur loss[73] or partial reduction to metallic Ni. In contrast, the Ni/C catalyst requires the complete reduction of the Ni^{2+} precursor to metallic Ni, for which higher temperatures (500 °C) are required.

The phase of the synthesized Ni_3S_2/C was examined by powder X-ray diffraction (PXRD), as shown in Fig. 1. The PXRD pattern exhibits characteristic peaks at 2θ values of 21.7°, 31.0°, 37.7°, 44.3°, 49.7°, and 55.1°, corresponding to the (010), (110), (111), (020), (120), and (121) planes, respectively. These reflections of Ni_3S_2/C are consistent with the heazlewoodite phase as a reference (JCPDS No. 01-071-1682).[74]

Raman spectra of the carbon support and Ni_3S_2/C composite exhibit the characteristic D band (~1350 cm^{-1}), associated with structural defects, and the G band (~1600 cm^{-1}), corresponding to graphitic sp^2 carbon domains (Fig. S2a). The carbon support shows an I_D/I_G ratio of 0.96, indicative for partially disordered activated carbon. After deposition of Ni_3S_2 nanoparticles, the I_D/I_G ratio slightly increases to 0.99, indicating a minor increase in structural disorder, while preserving the overall carbon framework.[75] Thermogravimetric analysis (TGA) demonstrates that both the support and the nickel sulfide catalyst are thermally stable below 400 °C. A noticeable mass loss is observed between 450 and 750 °C, attributable to carbon decomposition.[76]

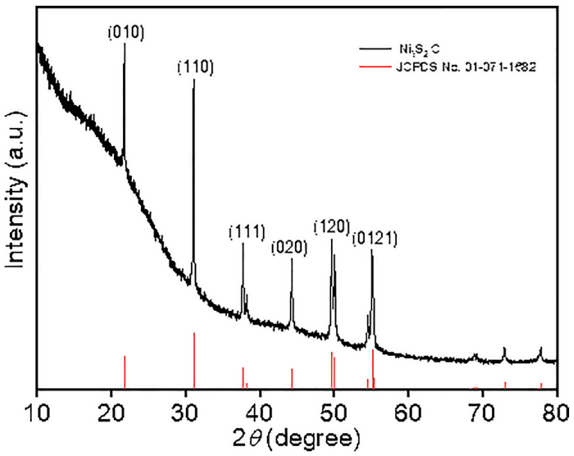

Fig. 1 Powder X-ray diffractogram of Ni_3S_2/C (10 wt% Ni).

To analyse the size, structure and composition of Ni_3S_2/C, transmission electron microscopy (TEM) was carried out (Fig. 2) and particles with an average size of 39 ± 5.2 nm (Fig. S1) were observed. High-resolution (HR)-TEM images show well-ordered lattice fringes over the whole nanoparticle. A *d*-spacing of 0.234 nm (Fig. 2b) corresponds to the (111) plane of bulk Ni_3S_2 as a reference.[74] Additionally, high-angle annular dark-field scanning (HAADF-S)TEM with energy-dispersive X-ray spectroscopy (EDXS) and element mapping (Fig. 2c–f) confirm a uniform distribution of Ni and S, and thus, of the active phase over the whole carbon support.

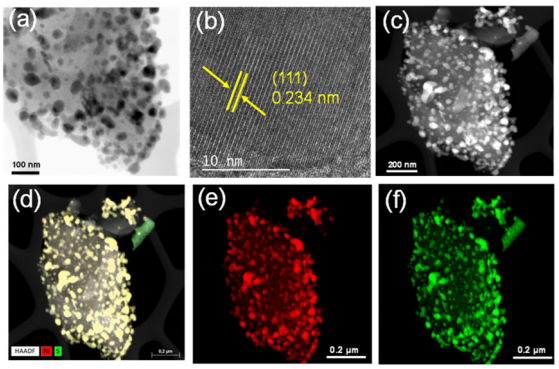

Fig. 2 (a) TEM overview image of Ni_3S_2/C (10 wt% of Ni). (b) HRTEM image of a single nanoparticle, showing lattice fringes. (c) HAADF-STEM image with (d–f) EDXS of nanoparticles on the HAADF-STEM image in (c) with element maps of (d) combined Ni and S, (e) Ni (red) and (f) S (green).

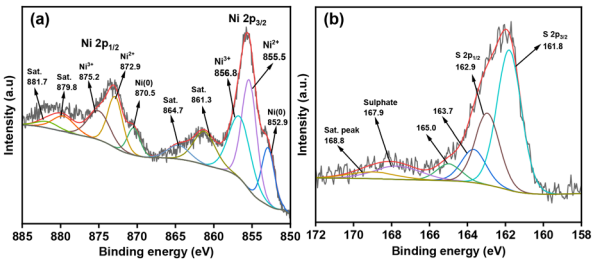

Fig. 3 XPS spectra of (a) Ni 2p and (b) S 2p regions of the Ni_3S_2/C catalyst.

To verify the elemental composition, inductively coupled plasma atomic emission spectroscopy (ICP-AES) was performed. The analysis shows 9 wt% Ni and 3 wt% S, and a total of 12 wt% of the active phase on carbon. These values are consistent with the theoretical stoichiometry of Ni_3S_2 (Ni : S = 3 : 2). An analysis of the specific surface area, following the Brunauer–Emmett–Teller (BET) approach, further confirms the successful incorporation of Ni_3S_2 onto the porous carbon matrix. The pristine carbon support exhibits a high surface area of 1319 $m^2\ g^{-1}$ and a pore volume of 0.60 mL g^{-1}, while the Ni_3S_2 loaded sample shows reduced values of 418 $m^2\ g^{-1}$ and 0.18 mL g^{-1}, respectively. This decrease indicates that Ni_3S_2 nanoparticles partially occupy/block the pores of the carbon support.

X-ray photoelectron spectroscopy (XPS) was employed to investigate the surface electronic structure of the Ni_3S_2/C catalyst (Fig. 3). The high-resolution Ni 2p spectrum (Fig. 3a) displays two primary spin-orbit doublets, corresponding to the Ni $2p_{3/2}$ and Ni $2p_{1/2}$ components. The peaks located at 855.5 and 872.9 eV are attributed to Ni^{2+} species, while the other peaks at 856.8 and 875.2 eV are assigned to Ni^{3+} species.[77] The signals at 852.9 and 870.5 eV correspond to metallic Ni^0.[78] Furthermore, the satellite signals observed at 861.3 and 864.7 eV in the Ni $2p_{3/2}$ region and at 879.8 and 881.7 eV in the Ni $2p_{1/2}$ region are characteristic shake-up satellite peaks associated with Ni^{2+} species. The high-resolution S 2p spectrum (Fig. 3b) exhibits a dominant doublet centred at 161.8 eV (S $2p_{3/2}$) and 162.9 eV (S $2p_{1/2}$), which is characteristic of S^{2-} species in Ni_3S_2/C. Additional peaks at 163.7 and 165.0 eV are attributed to surface polysulfide (S_n^{2-}) species. A weak peak at 167.9 eV is assigned to sulphate species, likely formed due to surface oxidation of sulphur upon exposure to air. This is a well-known observation for sulfide-based materials.[79] These results collectively confirm the presence of metal–sulphur bonding and are consistent with the characteristic electronic structure of Ni_3S_2 supported on carbon.

3.2. Catalytic transfer hydrogenation of nitrobenzene

The catalytic activity of the supported Ni_3S_2 catalysts (10 wt% Ni) was evaluated in the transfer hydrogenation of nitrobenzene to aniline using hydrazine monohydrate as the hydrogen source at 70 °C (Table 1). In the initial blank experiments, the reaction was conducted without a base and with carbon as the support (without any Ni) and no conversion was observed

Table 1 Catalyst screening in the transfer hydrogenation of nitrobenzene[a]

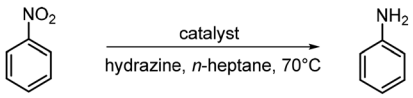

Entry	Catalyst	t (h)	Conversion (%)	Aniline yield (%)
1	Without catalyst	2	—	—
2	Carbon support	2	—	—
3	Ni_3S_2/SiO_2	2	74	15
4	Ni_3S_2/Al_2O_3	2	93	20
5	Ni_3S_2/ZrO_2	2	>99	26
6	Ni_3S_2/C	2	>99	64
7	Ni_3S_2/C	5	>99	85
8	Ni_3S_2/C	6	>99	91
9	Ni/C	2	>99	31
10	Ni/C	6	>99	54

[a] Reaction conditions: nitrobenzene (0.97 mmol, 0.1 mL), catalyst (30 mg, 10 wt% Ni), *n*-heptane (2 mL), 70 °C, and hydrazine monohydrate (10 equiv.). Conversions and yields were determined by GC-MS with *n*-decane as an external standard.

(Table 1, entries 1 and 2). This clearly indicates that the presence of a metal catalyst is essential for the transfer hydrogenation reaction.

Subsequently, various supported Ni_3S_2 catalysts were screened using different support materials, such as ZrO_2, Al_2O_3, and SiO_2. These catalysts enabled nitrobenzene conversions ranging from 74% to >99%, with aniline yields between 15 and 26% (Table 1, entries 3–5). Notably, Ni_3S_2 supported on carbon (Ni_3S_2/C) showed superior performance with respect to Ni_3S_2 on other support materials, achieving complete nitrobenzene conversion (>99%) and a 64% aniline yield within 2 h at 70 °C (Table 1, entry 6). Extending the reaction times to 5 and 6 h, respectively, further improved the aniline yield to 85% and 91% (Table 1, entries 7 and 8). For comparison, the reaction was also performed using a sulphur-free Ni/C catalyst (10 wt% Ni) as reference system, which resulted in complete nitrobenzene conversion, but only 31% aniline yield in 2 h (Table 1, entry 9). In this reaction, azobenzene and azoxybenzene were identified as by-products (Fig. S8). Although the aniline yield could be improved to 54% after 6 h with Ni/C, the sulphide-containing catalyst (Ni_3S_2/C) achieved a significantly higher yield of 91%, clearly outperforming the sulphur-free Ni/C reference catalyst (Table 1, entries 8 and 10). The productivity of aniline over the Ni_3S_2/C catalyst was calculated (at 6 h) to be 4.9 mmol $g^{-1}\ h^{-1}$, whereas the Ni/C catalyst exhibited a lower productivity of 2.9 mmol $g^{-1}\ h^{-1}$ under identical reaction conditions. This ~1.7-fold enhancement in productivity quantitatively highlights the crucial role of sulphur incorporation in improving catalytic performance for the transfer hydrogenation of nitrobenzene to aniline.

Given the exceptional catalytic performance of Ni_3S_2 on carbon in the transfer hydrogenation of nitrobenzene to aniline, it was selected as the catalyst for further reaction optimization studies. These investigations focused on the effects of reaction temperature, reaction time, amount of hydrazine monohydrate, and type of hydrogen donor (Fig. 4). Each reaction parameter was varied individually, while keeping other

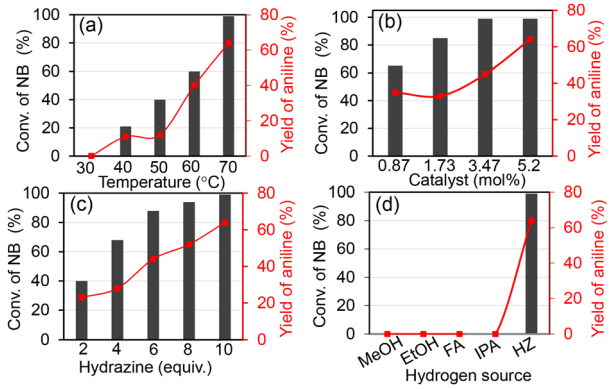

Fig. 4 Nitrobenzene conversion and aniline yield under different reaction conditions: (a) effect of temperature, (b) effect of catalyst amount, (c) effect of hydrazine amount, and (d) choice of the hydrogen source. NB: nitrobenzene, FA: formic acid, IPA: isopropanol and HZ: hydrazine.

reaction conditions constant to understand its sole influence on the catalytic performance.

Temperature optimization was carried out in the range of 30–70 °C using nitrobenzene as the model substrate and hydrazine monohydrate as the hydrogen source (Fig. 4a and Table S2). At 30 °C, no conversion was observed. Increasing the temperature to 40 °C resulted in 21% conversion of nitrobenzene. Further temperature increments from 40 to 70 °C led to progressively higher conversion rates and improved aniline yields.

To investigate the effect of catalyst amount, reactions were performed using varying amounts of Ni_3S_2/C (0.87–5.2 mol%) under standard reaction conditions (70 °C, 2 h, *n*-heptane as the solvent, Fig. 4b and Table S3). Using 0.87 mol% of catalyst resulted in a 65% nitrobenzene conversion and 35% yield of aniline. Increasing the catalyst amount to 1.73–5.2 mol% enhanced both conversion and aniline yield (33–64%), likely due to the greater availability of catalytically active Ni sites.

The influence of hydrazine monohydrate quantity was examined in the range of 2 to 10 equiv. (Fig. 4c and Table S4). Here, a direct correlation was observed between the amount of hydrazine and aniline yield, which increased from 23 to 64%. This improvement can be attributed to the greater availability of hydrogen gas, which accelerates the reduction of nitrobenzene and its intermediates. A higher hydrazine concentration also enhances reaction kinetics, suppresses side reactions leading to condensation by-products, and maintains a strongly reducing environment throughout the reaction.

Additionally, various other hydrogen donors were explored, including isopropanol, methanol, ethanol, formic acid, and hydrazine monohydrate (Fig. 4d and Table S5). Among these, only hydrazine monohydrate effectively facilitated the hydrogenation of nitrobenzene to aniline.

3.3. Mechanistic investigations

After optimizing the reaction parameters, time-dependent studies were conducted to identify possible intermediates during the transfer hydrogenation of nitrobenzene over Ni/C and Ni_3S_2/C as catalysts (Fig. 5).

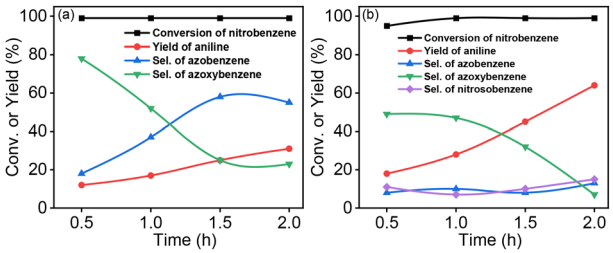

Fig. 5 Time-dependent reaction monitoring for the catalytic conversion of nitrobenzene over (a) Ni/C and (b) Ni_3S_2/C. Reaction conditions: nitrobenzene (1 mmol), catalyst (30 mg, 10 wt%), *n*-heptane (2 mL), 70 °C, hydrazine monohydrate (10 equiv.) and time (0.5–2 h). Conversion, selectivity and yield were calculated by GC-MS with *n*-decane as an external standard.

For Ni/C, extending the reaction time from 0.5 h to 2 h resulted in an increase in aniline yield and azobenzene selectivity, accompanied by a decrease in azoxybenzene selectivity. Notably, nitrosobenzene was not detected at any stage using Ni/C as the catalyst. In contrast, when the reaction was performed with Ni_3S_2/C, the yield of aniline increased steadily with time, while the selectivity of other intermediates remained largely unchanged. Interestingly, nitrosobenzene was consistently observed as an intermediate throughout the reaction over Ni_3S_2/C.

To further probe the mechanistic pathway, control experiments were carried out using nitrosobenzene and azobenzene as substrates under the before optimized reactions conditions (Scheme S1). When nitrosobenzene was used with Ni_3S_2/C as the catalyst, complete conversion was achieved in 2 h, yielding aniline (91%) and azobenzene (9%). Similarly, over Ni/C, nitrosobenzene was fully converted, producing aniline (82%) and azobenzene (18%). However, when azobenzene was used as the substrate, both catalysts exhibited sluggish activity, with only trace amounts of aniline being detected. These findings, combined with literature reports,[45] suggest that the reaction can proceed *via* two pathways: a direct pathway, involving nitrosobenzene and *N*-phenylhydroxylamine as intermediates, and a condensation pathway, which involves azoxybenzene and azobenzene (Fig. 6). Our results indicate that the reaction over Ni_3S_2/C proceeds mainly *via* a competitive pathway involving nitrosobenzene as an intermediate, whereas condensation

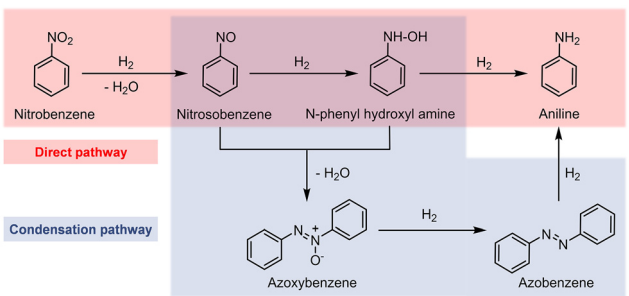

Fig. 6 Reaction pathway for catalytic transfer hydrogenation of nitrobenzene to aniline.

pathways are more prominent over Ni/C. Surprisingly, the incorporation of sulphur into the nickel lattice appears to play a crucial role in modulating the reaction pathway, thereby enhancing the aniline selectivity in the transfer hydrogenation of nitrobenzene.

3.4. Recyclability study and gram-scale reaction

The recyclability of the Ni_3S_2/C catalyst was evaluated under optimized reaction conditions during four consecutive reaction runs (Fig. 7). After each catalytic cycle, the catalyst was recovered by centrifugation, thoroughly washed with ethyl acetate and acetone, and dried before reuse. The results demonstrate that the catalyst can be recycled for up to four consecutive runs with only a slight decrease in activity.

The spent Ni_3S_2/C catalyst, recovered after the first catalytic cycle, was characterized by TEM, PXRD, and XPS to evaluate its bulk and surface stability. TEM analysis revealed only a marginal increase in average particle size from 39 to 40 nm, indicating negligible sintering during the reaction (Fig. S1 and S4). The PXRD pattern of the recovered catalyst showed no detectable phase transformation or formation of new crystalline phases, confirming the preservation of the bulk crystal structure under the reaction conditions (Fig. S5). Furthermore, XPS analysis of the Ni 2p and S 2p regions demonstrated that the surface chemical states of Ni and S species were retained after the reaction (Fig. S6). These findings correlate well with the stable catalytic performance observed during recycling experiments.

To assess the practical applicability of Ni_3S_2/C as the transfer hydrogenation catalyst, a gram-scale hydrogenation of nitrobenzene was performed by proportionally increasing all reaction components, including the catalyst amount (Scheme S2b). Here, the complete conversion of nitrobenzene (>99%) with 64% aniline yield was achieved in 2 h, which completely aligns with the small-scale reaction reported before. In the gram-scale reaction, the aniline yield could even be enhanced to 92% in 6 h reaction time (Scheme S2c). Under these conditions, the reaction proceeded efficiently, confirming the potential of Ni_3S_2/C as the catalyst for industrial-scale transfer hydrogenation processes.

3.5. Substrate scope

To evaluate the versatility of the Ni_3S_2/C catalyst, the transfer hydrogenation of various nitroarenes, bearing different functional groups, was investigated under optimized reaction conditions (Table 2). The catalyst showed excellent catalytic activity in the transfer hydrogenation of nitroarenes, containing both electron-donating and electron-withdrawing substituents, regardless of their steric hindrance (Table 2, entries 2–8). Also, halogen-substituted nitroarenes, which are typically prone to dehalogenation,[80] were selectively converted to the corresponding aromatic amines with high selectivity (>99%, Table 2, entries 6–8). The transfer hydrogenation of 1,4-dinitrobenzene also proceeded efficiently, affording complete conversion with 60% selectivity towards the desired product (Table 2, entry 9). Furthermore, nitroarenes with additional reducible groups, such as 4-nitrobenzonitrile, underwent the selective reduction of the nitro group to the corresponding amine with 94% selectivity (Table 2, entry 10). Particularly noteworthy is the hydrogenation of nitroarenes with sulphur-containing functional groups, which has been rarely explored in the field of heterogeneous catalysis, due to the strong chemisorption of sulphur atoms on metal surfaces and subsequent catalyst poisoning.[81] Despite this challenge, Ni_3S_2/C efficiently converted sulphur-containing nitroarenes into the corresponding amines (Table 2, entries 11–13). Interestingly, the Ni/C reference catalyst showed significantly lower activity for the hydrogenation of sulphur-containing nitroarenes, such as 4-nitrothioanisole, whereas Ni_3S_2/C achieved complete conversion with identical reaction conditions (Ni_3S_2/C: >99% conversion in 6 h *versus* Ni/C: 65% conversion in 6 h). These results highlight the robustness and high selectivity of Ni_3S_2/C as an efficient catalyst for the transfer hydrogenation of a broad range of nitroaromatic compounds.

A detailed comparison of the Ni_3S_2/C catalyst with previously reported systems is presented in Table S1. The analysis highlights several key advantages of Ni_3S_2/C over conventional catalysts. Ni_3S_2/C achieves complete conversion of nitrobenzene under mild reaction conditions (70 °C and atmospheric pressure), whereas many reported approaches require elevated temperatures, high hydrogen pressures, or noble metal catalysts, based on Pd, Pt, Ru, or Rh.[28–37] While Fe- and Co-based catalysts (*e.g.*, ImmFe-IL, FeS_2 NPs, Fe–Fe_3C–Fe_3O4@CN, Co@C/CNT, Co-L@C-800, and Co@NCT) often achieve complete conversion and high selectivity with hydrazine or other hydrogen donors, Ni-based systems typically require higher reaction temperatures.[44–46,48] When compared to the reported Ni_2P/AC system, Ni_2P/AC affords an aniline yield of 93% in 2 h in *n*-heptane, while Ni_3S_2/C initially reaches a lower aniline yield of 64% under comparable reaction conditions (Table S6).[46] However, extending the reaction time to 6 h increases the yield of Ni_3S_2/C to 91%, demonstrating that high aniline yield/selectivity can be achieved without compromising the mild operating conditions. Importantly, Ni_3S_2/C uniquely exhibits high catalytic activity toward sulphur-containing nitroarenes, a substrate class that has not been previously addressed by any Ni-based transfer hydrogenation catalysts, including Ni_2P/AC. This capability overcomes a well-known limitation of non-noble Ni catalysis and underscores the broad applicability and robustness of the herein reported Ni_3S_2/C.

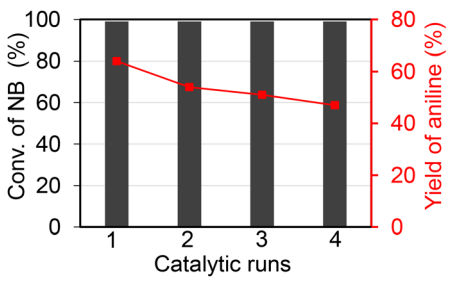

Fig. 7 Recyclability experiment for catalytic transfer hydrogenation of nitrobenzene to aniline. Reaction conditions: nitrobenzene (0.97 mmol), catalyst (30 mg, 10 wt%), *n*-heptane (2 mL), 70 °C, hydrazine monohydrate (10 equiv.), and 2 h. NB: nitrobenzene.

Table 2 Catalytic transfer hydrogenation of nitroarenes to corresponding amines over Ni_3S_2/C catalysts[a]

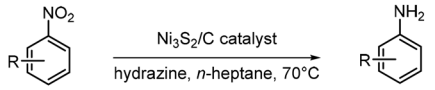

1a-m 2a-m

Entry	Substrate	t (h)	Conversion (%)	Product	Selectivity (%)
1	 1a	6	>99	 2a	91
2	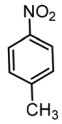 1b	6	>99	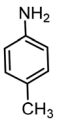 2b	>99
3	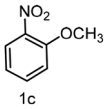 1c	6	>99	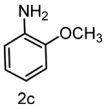 2c	>99
4	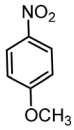 1d	9	95	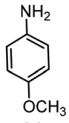 2d	>99
5	 1e	6	>99	 2e	>99
6	 1f	6	>99	 2f	>99
7	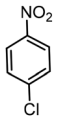 1g	7	>99	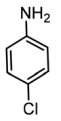 2g	>99
8	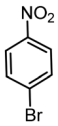 1h	6	>99	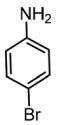 2h	>99
9	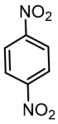 1i	6	>99	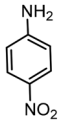 2i	60
10	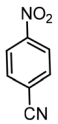 1j	6	>99	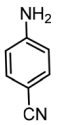 2j	94
11	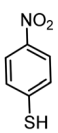 1k	6	>99	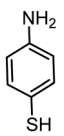 2k	>99
12	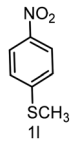 1l	6	>99	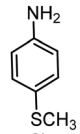 2l	>99
13	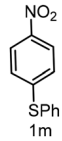 1m	6	>99	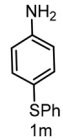 1m	>99

[a] Reaction conditions: substrate (1 mmol), catalyst (30 mg, 10 wt%), *n*-heptane (2 mL), 70 °C, and hydrazine monohydrate (10 equiv.). Conversions and selectivities were determined by GC-MS with *n*-decane as an external standard*.

4. Conclusions

This work establishes Ni_3S_2/C as an efficient and sustainable catalyst for the transfer hydrogenation of nitroarenes, using hydrazine monohydrate as the hydrogen source. The catalyst selectively reduces nitro groups in various aromatic substrates under mild reaction conditions, offering a practical alternative to conventional hydrogenation processes that rely on noble metals and molecular hydrogen. Mechanistic studies reveal that Ni_3S_2/C mainly promotes a direct reaction pathway from nitrobenzene to aniline, involving nitrosobenzene as a key intermediate, whereas Ni/C favours a condensation pathway *via* azoxybenzene and azobenzene. Control experiments confirmed the underlying reaction pathways and highlighted the critical role of sulphur incorporation into nickel when tuning the selectivity of transfer hydrogenation reactions towards aniline. Investigations of the substrate scope demonstrated the applicability of the system to a wide variety of nitroarene derivatives. Interestingly, Ni_3S_2/C significantly enhances sulphur resistance, as it also functions as a catalyst for the transfer hydrogenation of thiol-containing nitrobenzene. Beyond these insights, the catalyst demonstrated excellent recyclability, maintaining good activity over multiple catalytic cycles with minimal performance loss. Furthermore, a gram-scale hydrogenation of nitrobenzene to aniline was successfully performed, achieving complete conversion. This result underscores the industrial relevance and scalability of the Ni_3S_2/C based catalytic system. Compared to traditional catalyst systems, the presented Ni_3S_2/C catalyst is cost-effective and robust paving the way for broader adoption in fine chemical synthesis and pharmaceutical manufacturing. Future research will focus on expanding the substrate scope, exploring other sulphur-modified transition metal systems, and integrating this methodology into continuous-flow processes for large-scale applications.

Conflicts of interest

There are no conflicts to declare.

Data availability

Further information is available in the supplementary information (SI). Supplementary information is available. See DOI: https://doi.org/10.1039/d5ma01349f. Also, all additional data in open file formats has been uploaded in the NFDI4Cat Central Data Repository Repo4Cat (https://hdl.handle.net/21.11165/4cat/3edu-kaap).

Acknowledgements

We thank the Federal Ministry of Research, Technology and Space (BMFTR) for funding through the, CARBO-DIOL2.0 - Von Kohlenhydraten aus sekundären Rohstoffquellen zu Chemierohstoffen‘‘ project (project number: 03XP0612B). We thank Dr. Merve Kurt, Institute for chemical technology and polymer chemistry, KIT, for the Raman measurements. We would also like to thank Silvia Gross, University of Padova, for discussions regarding the XPS measurements.

Notes and references

1 Y. Chi, S. Zheng, X. Zhang and G. Li, *Int. J. Hydrogen Energy*, 2021, **46**, 36124–36136.
2 K. Murugesan, M. Beller and R. V. Jagadeesh, *Angew. Chem., Int. Ed.*, 2020, **59**, 17408–17412.
3 H. Miao, H. Shiwei, K. Ma, L. Sun, W. Fufang, H. Wang and H. Li, *Catal. Commun.*, 2018, **109**, 33–37.
4 Y. M. Yuan, J. Y. Long, H. Xiwei, X. Dan, Y. Zhu and Z. Dong, *ChemSusChem*, 2018, **11**, 4156–4165.
5 H. Lei, F. Tang, F. Hao, H. Zhao, W. Liu, Y. Lv, P. Liu, W. Xiong and H. Luo, *ACS Sustainable Chem. Eng.*, 2022, **10**, 2947–2959.
6 H. Qi, J. Yang, F. Liu, L. Zhang, J. Yang, X. Liu, L. Li, Y. Su, Y. Liu, R. Hao, A. Wang and T. Zhang, *Nat. Commun.*, 2021, **12**, 3295.
7 K. Murugesan, T. Senthamarai, V. G. Chandrashekhar, K. Natte, P. C. J. Kamer, M. Beller and R. V. Jagadeesh, *Chem. Soc. Rev.*, 2020, **49**, 6273–6328.
8 H. Wei, X. Liu, A. Wang, L. Zhang, B. Qiao, X. Yang, Y. Huang, S. Miao, J. Liu and T. Zhang, *Nat. Commun.*, 2014, **5**, 5634.
9 T. Irrgang and R. Kempe, *Chem. Rev.*, 2020, **120**, 9583–9674.
10 Q. Sun, N. Wang, T. Zhang, R. Bai, A. Mayoral, P. Zhang, Q. Zhang, O. Terasaki and J. Yu, *Angew. Chem., Int. Ed.*, 2019, **58**, 18570–18576.
11 X. Sun, A. I. Olivos-Suarez, D. Osadchii, M. J. V. Romero, F. Kapteijn and J. Gascon, *J. Catal.*, 2018, **357**, 20–28.
12 Z. An, P. Yang, D. Duan, J. Li, T. Wan, Y. Kong, S. Caratzoulas, S. Xiang, J. Liu, L. Huang, A. I. Frenkel, Y. Y. Jiang, R. Long, Z. Li and D. G. Vlachos, *Nat. Commun.*, 2023, **14**, 6666.
13 M. Pang, J. Y. Chen, S. Zhang, R. Z. Liao, C. H. Tung and W. Wang, *Nat. Commun.*, 2020, **11**, 1249.
14 D. Zhang, X. Gao, T. Cheng and G. Liu, *Sci. Rep.*, 2014, **4**, 5091.
15 F. Wang, Z. Zhang, Y. Chen, V. Ratovelomanana-Vidal, P. Yu, G. Q. Chen and X. Zhang, *Nat. Commun.*, 2022, **13**, 7794.
16 F. Wang, O. Planas and J. Cornella, *J. Am. Chem. Soc.*, 2019, **141**, 4235–4240.
17 P. Hauwert, R. Boerleider, S. Warsink, J. J. Weigand and C. J. Elsevier, *J. Am. Chem. Soc.*, 2010, **132**, 16900–16910.
18 M. Subaramanian, G. Sivakumar, V. G. Landge, R. Kumar, K. Natte, R. V. Jagadeesh and E. Balaraman, *J. Catal.*, 2023, **425**, 386–405.
19 Y. Wei, Y. Liang, R. Luo and L. Ouyang, *Org. Biomol. Chem.*, 2023, **21**, 7484–7497.
20 V. Goyal, T. Bhatt, C. Dewangan, A. Narani, G. Naik, E. Balaraman, K. Natte and R. V. Jagadeesh, *J. Org. Chem.*, 2023, **88**, 2245–2259.
21 J. Wang, A. D. Ebner and J. A. Ritter, *J. Am. Chem. Soc.*, 2006, **128**, 5949–5954.
22 J. Graetz, J. Wegrzyn and J. J. Reilly, *J. Am. Chem. Soc.*, 2008, **130**, 17790–17794.
23 W. Zhao, H. Li, H. Zhang, S. Yang and A. Riisager, *Green Energy Environ.*, 2023, **8**, 948–971.
24 D. Cantillo, M. M. Moghaddam and C. O. Kappe, *J. Org. Chem.*, 2013, **78**, 4530–4542.
25 M. G. Kallitsakis, K. D. Nikopoulos and I. N. Lykakis, *ChemCatChem*, 2025, **17**, e202401927.
26 V. Dragutan, I. Dragutan, L. Delaude and A. Demonceau, *Coord. Chem. Rev.*, 2007, **251**, 765–794.
27 S. Enthaler, R. Jackstell, B. Hagemann, K. Junge, G. Erre and M. Beller, *J. Organomet. Chem.*, 2006, **691**, 4652–4659.
28 H. Liao, P. Weng, H. Huang, R. Tan, R. Zhu, Y. Liu and Z. Wang, *RSC Adv.*, 2023, **13**, 20876.
29 V. Goyal, N. Sarki, M. K. Poddar, A. Narani, D. Tripathi, A. Ray and K. Natte, *New J. Chem.*, 2021, **45**, 14687–14694.
30 Q. Liu, H. Fu, W. Wang, L. Zhu, Y. Fang, Z. Yang, A. Kroner, H. Ye and B. H. Chen, *ACS Appl. Nano Mater.*, 2024, **7**, 22517–22524.
31 J. Li, S. Wang, Z. Yu, H. Zhang, L. Zhu, C. Wu and H. Yu, *Ind. Eng. Chem. Res.*, 2025, **64**, 10844–10851.
32 X. Shi, X. Wang, X. Shang, X. Zou, W. Ding and X. Lu, *ChemCatChem*, 2017, **9**, 3743–3751.
33 V. Goyal, N. Sarki, K. Natte and A. Ray, *J. Ind. Chem. Soc.*, 2021, **98**, 100014.
34 Q. Zhang, J. Bu, J. Wang, C. Sun, D. Zhao, G. Sheng, X. Xie, M. Sun and L. Yu, *ACS Catal.*, 2020, **10**, 10350–10363.
35 Y. Qu, H. An, X. Zhao and Y. Wang, *Chem. Eng. J.*, 2024, **496**, 153949.
36 Y. Zhang, L. J. Zhou, F. Wang and X. Zhao, *Langmuir*, 2022, **38**, 7699–7708.
37 H. Tian, J. Zhou, Y. Li, Y. Wang, L. Liu, Y. Ai, Z. N. Hu, J. Li, R. Guo, Z. Liu, H. Sun and Q. Liang, *ChemCatChem*, 2019, **11**, 5543–5552.
38 J. Yu, X. Zhang, R. Jiang, W. He, M. Xu, X. Xu, Q. Xiang, C. Yin, Z. Xiang, C. Ma, Y. Liu, X. Li and C. Lu, *ACS Appl. Mater. Interfaces*, 2024, **16**, 8603–8615.

39 X. Zheng, B. Li, R. Huang, W. jiang, L. Shen, G. Lei, S. Wang, Y. Zhan and L. Jiang, *ACS Catal.*, 2024, **14**, 10245–10259.
40 N. Sarki, R. Kumar, B. Singh, A. Ray, G. Naik, K. Natte and A. Narani, *ACS Omega*, 2022, **7**, 19804–19815.
41 X. Li, R. Sun, L. Zhao, J. Wang, Z. Wang, W. Li and X. Wang, *Appl. Organomet. Chem.*, 2025, **39**, e7974.
42 N. M. Patil, T. Sasaki and B. M. Bhanage, *ACS Sustainable Chem. Eng.*, 2016, **4**, 429–436.
43 J. P. Southouse, L. Lazzarin, A. O. Ibhadon and M. Grazia Francesconi, *New J. Chem.*, 2021, **45**, 17808–17815.
44 K. J. A. Raj, M. G. Prakash, R. Mahalakshmy, T. Elangovan and B. Vishwanathan, *Chin. J. Catal.*, 2012, **33**, 1299–1305.
45 Y. Qu, H. Yang, S. Wang, T. Chen and G. Wang, *Catal. Commun.*, 2017, **97**, 83–87.
46 F. Yang, M. Wang, W. Liu, B. Yang, Y. Wang, J. Luo, Y. Tang, L. Hou, Y. Li, Z. Li, B. Zhang, W. Yang and Y. Li, *Green Chem.*, 2019, **21**, 704–711.
47 D. Sharma, P. Choudhary, S. Kumar and V. Krishnan, *J. Colloid Interface Sci.*, 2024, **657**, 449–462.
48 C. Jiang, Z. Shang and X. Liang, *ACS Catal.*, 2015, **5**, 4814–4818.
49 K. Martina, M. J. Moran, M. Manzoli, M. V. Trukhan, S. Kuhn, T. V. Gerven and G. Cravotto, *Org. Process Res. Dev.*, 2024, **28**, 1515–1528.
50 Y. Zhou, A. Guo, H. Shen, Y. Wang, F. Zhang, X. Rong, Y. Li, X. Yan, L. Chen and B. Wang, *ChemCatChem*, 2025, **17**, e202401902.
51 G. Zhang, L. Liu, Q. Zhu and X. Kong, *Catal. Lett.*, 2023, **153**, 1536–1542.
52 Z. Zhang, Y. Liu, J. Du, Y. Jiang, Z. Wang, R. Yun and B. Zheng, *Inorg. Chem. Front.*, 2023, **10**, 7028–7037.
53 S. Dey, S. D. Thakur, A. Sau, D. Panja, T. Roy, J. Zhang, H. V. Annadata and S. Kundu, *J. Catal.*, 2024, **439**, 115759.
54 S. Dey, D. Panja, A. Sau, S. D. Thakur and S. Kundu, *J. Org. Chem.*, 2023, **88**, 10048–10057.
55 H. Jin, P. Li, P. Cui, J. Shi, W. Zhou, X. Yu, W. Song and C. Cao, *Nat. Commun.*, 2022, **13**, 1–9.
56 V. Goyal, N. Sarki, B. Saint, A. Ray, M. Poddar, A. Bordoloi, A. Narani and K. Natte, *ACS Appl. Nano Mater.*, 2020, **3**, 11070–11079.
57 Z. Ma, J. Chen, M. Chen, L. Dong, W. Mao, Y. Long and J. Ma, *ChemCatChem*, 2024, **16**, e202400336.
58 M. Yuan, Y. Long, J. Yang, X. Hu, D. Xu, Y. Zhu and Z. Dong, *ChemSusChem*, 2018, **11**, 4156–4165.
59 S. Hanf, L. A. Rupflin, S. Iqbal, R. Gläser and S. A. Schunk, *catalysts*, 2020, **10**, 510.
60 L. Karam, C. Fares, C. Weidenthaler and N. Neumann, *Angew. Chem., Int. Ed.*, 2024, **63**, e202404292.
61 Z. Zhao and Z. Y. Yuan, *Smart Mater. Devices*, 2025, **1**, 202521.
62 A. Neyyathala, F. Flecken, F. Rang, C. Papke and S. Hanf, *Chem. – Eur. J.*, 2024, **30**, e202302825.
63 A. Neyyathala, F. Flecken and S. Hanf, *ChemPlusChem*, 2023, **88**, e202200431.
64 H. Ishikawa, S. Yamaguchi, A. Nakata, K. Nakajima, S. Yamazoe, J. Yamasaki, T. Mizugaki and T. Mitsudome, *JACS Au*, 2022, **2**, 419–427.
65 J. N. D. Leon, C. R. Kumar, J. A. Garcia and S. F. Moyado, *Catalysts*, 2019, **9**, 87.
66 L. Gong, W. Zhang, Y. Zhuang, K. Zhang, Q. Zhao, D. Xiao, S. Liu, Z. Liu and Y. Zhang, *ACS Appl. Mater. Interfaces*, 2024, **16**, 66211–66218.
67 A. Neyyathala, E. Faco, S. De, D. Gashnikova, F. Maurer, J. D. Grunwaldt, S. A. Schunk and S. Hanf, *Small Struct.*, 2025, **6**, 2400260.
68 X. Lin, M. Zhang., X. Liu, J. Liu, H. Dai, W. Luo, J. Liu, R. Cao and Q. Yang, *ACS Catal*, 2024, **14**, 16214–16223.
69 I. Sorribes, L. Liu and A. Corma, *ACS Catal.*, 2017, **7**, 2698–2708.
70 L. Lückemeier, T. D. Vos, L. Schlichter, C. Gutheil, C. G. Daniliuc and F. Glorius, *J. Am. Chem. Soc.*, 2024, **146**(9), 5864–5871.
71 Q. Zhang, W. Xu, X. Li, D. Jiang, Y. Xiang, J. Wang, J. Cen, S. Romano and J. Ni, *Appl. Catal. A*, 2015, **497**, 17–21.
72 Z. Y. Wu, H. Nan, S. C. Shen, M. X. Chen, H. W. Liang, C. Q. Huang, T. Yao, S. Q. Chu, W. X. Li and S. H. Yu, *CCS Chem.*, 2022, **4**, 3051–3063.
73 A. Neyyathala, E. Fako, S. De, D. Gashnikova, F. Maurer, J. D. Grunwaldt, S. A. Schunk and S. Hanf, *Small Struct.*, 2025, **6**, 2400260.
74 M. Kumar, D. I. Jeong, N. Sarwar and D. H. Yoon, *Ceram. Int.*, 2021, **47**, 16852–16860.
75 Z. Liu, Y. Sun, X. Xu, J. Qu and B. Qu, *ACS Omega*, 2020, **5**, 29231–29242.
76 S. Sharma, M. Kaur, C. Sharma, A. Choudhary and S. Paul, *ACS Omega*, 2021, **6**, 19529–19545.
77 J. Tang, S. Ni, D. Chao, J. Liu, X. Yang and J. Zhao, *Electrochim. Acta*, 2018, **265**, 709–716.
78 J. Zhang, T. Wang, P. Liu, Z. Liao, S. Liu, X. Zhuang, M. Chen, E. Zschech and X. Feng, *Nat. Commun.*, 2017, **8**, 15437.
79 X. Liu, Y. Li, N. Chen, D. Deng, X. Xing and Y. Wang, *Electrochim. Acta*, 2016, **213**, 730–739.
80 J. Li, S. Ding, F. Wang, H. Zhao, J. Kou, M. Akram, M. Xu, W. Gao, C. Liu, H. Yang and Z. Dong, *J. Colloid Interface Sci.*, 2022, **625**, 640–650.
81 X. Liu, Y. Ren, M. Wang, X. Ren, J. Liu and Q. Yang, *ACS Catal.*, 2022, **12**, 11369–11379.